A general framework for denoising phaseless diffraction measurements

Huibin Chang, Stefano Marchesini

***Abstract*—We propose a general framework to recover underlying images from noisy phaseless diffraction measurements based on the alternating directional method of multipliers and the plug-and-play technique. The algorithm consists of three-step iterations: (i) Solving a generalized least square problem with the maximum a posteriori (MAP) estimate of the noise, (ii) Gaussian denoising and (iii) updating the multipliers. The denoising step utilizes higher order filters such as total generalized variation and nonlocal sparsity based filters including nonlocal mean (NLM) and Block-matching and 3D filtering (BM3D) filters. The multipliers are updated by a symmetric technique to increase convergence speed. The proposed method with low computational complexity is provided with theoretical convergence guarantee, and it enables recovering images with sharp edges, clean background and repetitive features from noisy phaseless measurements. Numerous numerical experiments for Fourier phase retrieval (PR) as coded diffraction and ptychographic patterns are performed to verify the convergence and efficiency, showing that our proposed method outperforms the state-of-art PR algorithms without any regularization and those with total variational regularization.**

***Index Terms*—Phaseless diffraction measurements, Ptychographic phase retrieval, coded diffraction pattern, image denoising, ADMM, BM3D**

I. Introduction

PHase retrieval (PR) plays a central role in the X-ray diffraction imaging in vast industrial and scientific applications, such as crystallography and optics in [1], [2], [3], [4], [5], *etc*, and its goal is to reconstruct an object from phaseless measurements, *i.e.* only pointwise magnitudes of the Fourier transform (FT) of the object are available. Throughout the paper we discuss the PR from the noisy phaseless measurements in a discrete setting.

Assume we have an underlying 2-dimensional unknown object u with $n_1 \times n_2$ pixels. We denote u in terms of a vector of size $n = n_1 \times n_2$ by a lexicographical order, i.e.

$$u : \Omega = \{0, 1, \cdots, n-1\} \to \mathbb{C}.$$

We call classical PR problem [6] when one is given the magnitudes of the Fourier transform of u, *i.e.*, $|\mathcal{F}u|^2$, where $|\cdot|^2$ denotes the pointwise square of the absolute value of a vector, and $\mathcal{F} : \mathbb{C}^n \to \mathbb{C}^n$ denotes the discrete Fourier transform (DFT), and the problem consists of retrieving the underlining image u. A general PR problem [7], [8] can be obtained as follows

$$\text{To find} \quad u \in \mathbb{C}^n, \quad s.t. \quad |\mathcal{A}u|^2 = b,$$

with the phaseless measurement $b : \tilde{\Omega} = \{0, 1, \cdots, m-1\} \to \mathbb{R}_+$, if one can extend the DFT operator $\mathcal{F}$ to arbitrary linear operator $\mathcal{A} : \mathbb{C}^n \to \mathbb{C}^m$.

The measurements can be contaminated by noise, or miscalibration of the experimental geometry, or the illumination mask, which leads to further trouble for the algorithm design. Generally speaking, PR involves solving a quadratic inverse problem, which is ill-posed and challenging. Here we give a brief review for the computational tools for it. In 1947 D. Gabor [9] combined a known "reference" signal which linearized the PR problem, and received the Noble prize in Physics in 1971, in the 1950s Karle and Hauptman [10], as well as Sayre [11] developed methods to solve the PR problem for binary atomic crystals. Hauptman and Karle received the Nobel prize in Chemistry in 1985. In earlier work, phaseless measurements of X-ray and electron diffraction played a pivotal role in unequivocally showing the existance of atoms [12], atomic structure of crystals by the Braggs, molecular components of life including DNA, and later RNA, and over 100,000 proteins structures to date awarded by more than 10 nobel prizes in physics, chemistry and biology. In 1969 Hoppe [13] proposed to use multiple diffraction measurements from a scanning sample, and in 1990s Rodemburg, Bates, and Chapman independently experimentally demonstrated a linearized inversion scheme based on the Wigner Distribution Deconvolution method [14], [15]. The complexities of the Wigner Deconvolution method are very high, which is about the square of the number of unknowns, and therefore it has not gained popularity in the experimental community. In 1972 Gerchberg and Saxton [16], introduced an alternating projection algorithm for a problem whereby one records phaseless measurements of the the scattering amplitude, and sample transmission. Fienup extended the method and applied it to the classical phase retrieval problem [17]. The connection between Fienup' Hybrid Input Output and the Douglas-Rachford algorithm was discussed in [18], [19], and the connection between the Douglas-Rachford and the ADM algorithm was discussed in [6]. Several variant heuristic algorithms popular in the optics community including [20], [21] were proposed to solve the classical PR problems, and one can refer to [22], [6] and the reference therein. These methods use projections onto nonconvex constraint set, and therefore it is very difficult to ensure the convergence theoretically. Recently, more work has

H. Chang is with Department of Mathematical Sciences, Tianjin Normal University, Tianjin, 300387 China, e-mail:changhuibin@gmail.com. He is currently a visiting scholar of the Center For Applied Mathematics for Energy Research Applications at Lawrence Berkeley National Laboratory.

S. Marchesini is with Computational Research Division, Lawrence Berkeley National Laboratory, Berkeley.

focused on the convergence theory. A global convergence for Gaussian measurements was analyzed by Netrapalli *et al.* [23]. The convergence under a generic frame was proved in [24], and spectral methods including initialization by truncation phase synchronization and framewise phase-synchronization were employed to accelerate projection methods for large scale ptychographic PR. Newton-type algorithms were proposed by Qian *et al.* [25] and Zhong *et al.*[26] to accelerate the convergence. A modified Levenberg-Marquardt method was proposed [27] with global convergence guarantees. A Wirtinger flow (WF) approach was proposed in [28] by comprised of an initialization by spectral method and gradient descent, and was further improved by truncated Wirtinger flow (TWF) [29]. A Douglas-Rachford (DR) algorithm for PR with oversampling measurements was proved to be locally and geometrically convergent by Chen and Fannjiang [30]. In order to deal with the conventional nonconvex projection algorithms for PR, the PhaseLift [31] algorithm was proposed by Candés *et al.* with the lift technique of semi-definite programming(SDP). The PhaseCut algorithm was proposed by Waldspurger *et al.* [7], where the PR problem was convexified by separating phases and magnitudes. A computationally tractable low-rank factorization method using lift technique of SDP was proposed in [32] for solving ptychographic PR.

Sparse prior information of the unknown u can be efficiently incorporated into PR in order to increase the quality of reconstructed image, especially when the data is noisy and incomplete. The SHRINK-WRAP algorithm generalized the regression model by slowly shrinking the size of the support of non-zero coefficients of u [33] and has been applied to several ground breaking experiments using X-ray Free Electron Lasers [34]. Similar methods based on hard thresholding, inversion [35], and L_1 soft thresholding have been proposed over the years, e.g. [36], [37]. SDP-based methods were proposed to solve a sparse PR problem [38], [39]. Directly extension of the Fieup's method [17] was proposed in [40] by an additional sparsity constraint of the L_0 norm for u. The L_1 regularization based variational method [41] was applied to the classical PR problem. An efficient local search method for recovering a sparse signal for the classical PR was presented in [42]. A probabilistic method based on the generalized approximate message passing algorithm was proposed in [43]. The shearlet and total variation sparsity regularization methods were considered in [44], [45], [46] by assuming the objects possess a sparse representation in the transform domain. Dictionary learning methods were proposed to reconstruct the image in [47], [48], where a dictionary was automatically learned from the redundant image patches.

In this paper, we consider the PR problem for the sparse images $u \in \mathbb{C}^n$ (or $\mathbb{R}^n$) in which the measured data $f \in \mathbb{R}_+^m$ are corrupted due to severe noisy measurements as

$$f = \mathrm{Corrupt}(|\mathcal{A}u|^2),$$

and a general minimization problem driven by regularization method of the underlying image can be established as

$$\min_u \Upsilon(u) := \mathbf{B}(|\mathcal{A}u|^2, f) + \lambda \mathbf{R}(u), \quad s.t.\ u \in \mathscr{K} \qquad (1)$$

where $u \in \mathscr{K}$ is an underlying image that we want to reconstruct from magnitude data f, $\mathbf{R}(u)$ is the sparse promoted term, $\mathbf{B}(|\mathcal{A}u|^2, f)$ is the data fitting term deduced by the maximum a posteriori (MAP) of the noise distribution, λ is the positive parameter to balance the sparsity and data fitting terms. Note that the set $\mathscr{K}$ is introduced to add some condition as positivity [5] or the box constraint [45] and support set. Stimulated by the alternating directional method of multipliers [49], [50] (ADMM) and the plug-and-play technique [51], [52], we reformulate it to a novel framework for PR with theoretical convergence guarantee, which consist of three steps: Solving a generalized least square problem with the maximum a posteriori (MAP) estimate of the noise, Gaussian denoising and updating the multipliers. In order to implement the denoising step, we utilize the higher order total variation such as total generalized variation and nonlocal sparsity based filters including nonlocal mean and Block-matching and 3D filtering (BM3D) filters in order to further improve the image quality compared with the work in [44], [45], [46]. Moreover, a symmetric technique is applied to the multiplier updating to order to increase the convergence speed.

The rest of this paper is organized as follows. In section II, we will show the general framework starting from the ADMM for solving (1). In section III, detailed numerical algorithms will be given, and the convergence of the proposed method is proved as well. In section IV, the numerical experiments are performed to demonstrate the effectiveness of the proposed methods. Conclusions and future works are given in section V.

II. General framework

A. MAP of noise

We consider two important types of noise as Poisson and Guassian noise. The measurements are usually contaminated by the Poisson noise for photon-counting, which follow Poisson distribution as follows

$$\mathrm{Pr}_\mu(n) = \frac{e^{-\mu}\mu^n}{n!}, \qquad n \geq 0,$$

where μ is the mean and standard deviation. The counted number of photons at pixel located at index i, denoted as $f(i)$, follows i.i.d. Poisson distributions with $h(i)$ being the ground-truth value as

$$f(i) \overset{\text{ind.}}{\sim} \mathrm{Poisson}(h(i)),\ \forall i \in \tilde{\Omega}. \qquad (2)$$

By MAP for a clean image h, the denoising problem can be expressed as $\max \mathrm{Pr}(h(i)|f(i))$ if f is measured. One can readily have

$$\mathrm{Pr}(h(i)|f(i)) = \frac{\mathrm{Pr}(f(i)|h(i))\mathrm{Pr}(h(i))}{\mathrm{Pr}(f(i))}, \qquad (3)$$

according to the Bayes' Law, and as a result, maximization of $\mathrm{Pr}(g(i)|f(i))$ is equivalent to maximization of $\mathrm{Pr}(f(i)|g(i))\mathrm{Pr}(g(i))$. Therefore, we have

$$\mathrm{Pr}(f(i)|h(i)) = \mathrm{Pr}_{h(i)}(f(i)) = \frac{e^{-h(i)}h(i)^{f(i)}}{(f(i))!}.$$

Finally, one should minimize the logarithm of the $\Pr(f(i)|h(i))\Pr(h(i))$ instead, *i.e.*

$$\begin{aligned}&\min_{h\geq 0}\sum_{i\in\tilde{\Omega}} -\log\Pr(f(i)|h(i)) - \log\Pr(h(i))\\ =&\min_{h\geq 0}\sum_{i\in\tilde{\Omega}}(h(i) - f(i)\log h(i)) - \log\Pr(h(i)).\end{aligned}$$

In a similar manner by replacing the Poisson distribution with Gaussian distribution, one can readily get the MAP of it, and we summarize them as follows

$$\mathbf{B}(h,f) := \begin{cases}\frac{1}{2}\langle h - f\log h, \mathbf{1}\rangle, & \text{for Poisson noised } f;\\ \frac{1}{2}\|h-f\|^2, & \text{for Gaussian noised } f,\end{cases} \tag{4}$$

where $\mathbf{1}$ denotes a vector whose entries are all one, and $\langle\cdot,\cdot\rangle$ denotes the L^2 inner product of two vectors.

B. General framework for PR

Regularization often plays an important role for noise removal, and therefore, one can establish a general model (1) if the measurements are collected from PR based on the above MAP. We will show how to build up a general framework starting from the ADMM step by step.

As a very popular solver, ADMM is simple and efficient to solve the existing variation models for noise removal. It can be obtained by introducing an auxiliary variable $\boldsymbol{p} = \nabla u$ as [45], [46] to prevent directly solving a non-differential minimization problems by splitting technique. However, in order to solve (1), there is an equivalent form to formulate the ADMM, which can provide a quite different understanding of the algorithm as [51]. By introducing an auxiliary viable $u = v$, one can readily decouple the data fitting term and regularization term as follows:

$$\begin{aligned}&\min_{u,v}\mathbf{B}(|\mathcal{A}u|^2, f) + I_{\mathscr{K}}(u) + \lambda\mathbf{R}(v),\\ &\quad s.t. \qquad u = v,\end{aligned} \tag{5}$$

where the indicator function $I_{\mathscr{K}}(u)$ defined by

$$I_{\mathscr{K}}(u) = \begin{cases} 0, & u\in\mathscr{K};\\ +\infty, & \text{otherwise},\end{cases}$$

with constrained set $\mathscr{K}$.

In order to solve (5), the corresponding augmented Lagrangian is introduced with the multiplier Λ as

$$\begin{aligned}\mathcal{L}_r(u,v;\Lambda) =&\mathbf{B}(|\mathcal{A}u|^2, f) + I_{\mathscr{K}}(u) + \lambda\mathbf{R}(v)\\ &+\mathrm{Re}(\langle u-v,\Lambda\rangle) + \frac{r}{2}\|u-v\|^2,\end{aligned} \tag{6}$$

where the parameter r is a positive constant, and $\mathrm{Re}(\cdot)$ denotes the real part of a complex-valued number. The ADMM with symmetric updating scheme following [53] can be written in order to solve the saddle point problem

$$\max_{\Lambda}\min_{u,v}\mathcal{L}_r(u,v;\Lambda)$$

as

$$\begin{cases} u^{k+1} = \arg\min_u \mathcal{L}_r(u, v^k; \Lambda^k),\\ \Lambda^{k+1/2} = \Lambda^k + r(u^{k+1} - v^k),\\ v^{k+1} = \arg\min_v \mathcal{L}_r(u^{k+1}, v; \Lambda^{k+1/2}),\\ \Lambda^{k+1} = \Lambda^{k+1/2} + r(u^{k+1} - v^{k+1}),\end{cases} \tag{7}$$

if provided with the kth iterative solution (u^k, v^k, Λ^k). The above algorithm is slightly different to [53] since a relax parameter for the step size r can not accelerate the convergence based on the numerical experiments reported in [53] and therefore we omit it for simplicity. In our numerical experiments, updating the multiplier with symmetric style can indeed speedup the proposed method (see details in Figure 14) compared with asymmetric style.

Let us analyze the first and the third subproblems one by one. First for the first subproblem, one needs to solve

$$\begin{aligned}u^{k+1} =& \arg\min_u \mathcal{L}_r(u, v^k; \Lambda^k)\\ =& \arg\min_u \mathbf{B}(|\mathcal{A}u|^2, f) + I_{\mathscr{K}}(u) + \frac{r}{2}\|u - (v^k - \Lambda^k/r)\|^2,\end{aligned}$$

which we call it a generalized least square minimization problem with respect to u with data term as $v^k - \frac{\Lambda^k}{r}$ in order to satisfy the statistical property of the noise. Similarly, for the third subproblem with respect to the variable v,

$$v^{k+1} = \arg\min_v \lambda\mathbf{R}(v) + \frac{r}{2}\|v - (u^{k+1} + \Lambda^{k+1/2}/r)\|^2, \tag{8}$$

which we call it a denoising step in order to smooth the data $u^{k+1} + \Lambda^{k+1/2}/r$. If setting $\mathbf{R}(v) = \mathrm{TV}(v)$, the well-known total variation [54], [55], [56], [57] based model was considered in for Gaussian noised data in [45] and Poisson noised data in [46].

Naturally one can build other generalized least square forms in the first subproblem by the maximum a posteriori (MAP) estimate for other kinds of noise, and in this paper we only focus on the Gaussian and Poisson noise, which are common and challengeable for PR. One can also generalize the third step by arbitrary variational denoising method such as higher order TV [58], [59], [60] instead of the traditional TV in order to promote the sparsity. Moreover, similar to the work in [61], [51], [52], some advanced filters as BM3D can be introduced to replace the variational image denoising methods. Therefore the proposed general framework is written in a unified form as

$$\begin{cases} \text{Step 1:} & u^{k+1} = \mathrm{Prox}_{\mathbf{G}/r + I_{\mathscr{K}}}\left(v^k - \frac{\Lambda^k}{r}\right),\\ \text{Step 2:} & \Lambda^{k+1/2} = \Lambda^k + r(u^k - v^{k+1}),\\ \text{Step 3:} & v^{k+1} = \mathrm{Prox}_{\sigma\mathbf{R}}\left(u^{k+1} + \frac{\Lambda^{k+1/2}}{r}\right),\\ \text{Step 4:} & \Lambda^{k+1} = \Lambda^{k+1/2} + r(u^{k+1} - v^{k+1}),\end{cases} \tag{9}$$

where the proximal operator is denoted as

$$\mathrm{Prox}_s(v) = \min_u s(u) + \frac{1}{2}\|u - v\|^2,$$

the operator $\mathrm{Prox}_{\sigma\mathbf{R}}$ denoises the data v, the noise level is directly denoted by $\sigma := \frac{\lambda}{r}$ in [62], and

$$\mathbf{G}(u) := \mathbf{B}(|\mathcal{A}u|^2, f).$$

In this paper, we will consider to implement this framework in two aspects. First, we consider two different data fitting terms of $\mathbf{B}(\cdot,\cdot)$ for the Poisson and Gaussian noise removal respectively. Second, for the denosing procedure in Step 3, two kinds of operators can be employed: One is the variational models with the explicit expression of $\mathbf{G}$ as ROF [57], LLT [63], nonlocal TV [64] and total generalized variation (TGV) [59]; The other kind is the filter based without the explicit expression of $\mathbf{R}$ such as the bilateral filter [65], nonlocal means filter (NLM) [66], and BM3D filter [67]. Our proposed method is rather simple and flexible, and can transform the denoising the noisy PR to traditional PR task (without regularization or filter) and the image denoising task. Therefore, a group of denoising methods can be employed to further improve the start-of-art PR methods. It will be very efficient, since we combine some advanced filters, and on this sense, we introduce a group of new filters for PR.

C. Connection with other related methods for PR

Our proposed method belongs to the "black box" methods. One do not need to specifically design elaborate algorithms for the original optimization models, and only focus on designing efficient solvers for subproblems. Actually similar ideas already exist in [61], [52], [68] where a general framework for image deblurring and inpainting in image and transform domains were proposed. Compared with the work [45], [46], one can design different and more efficient algorithm for the inner loop for the Step 1 and Step 3 of our proposed method to solve the generalized least square and image denoising problems. Compared with the work [47], [48], more fast and efficient filter as BM3D can be incorporated for the denoising step in our framework, and furthermore Poisson noised data can be dealt with by our proposed method. In a recent work in [69], a general framework was also proposed based on generalized approximate message passing from noisy data. However, they consider a different problem with measurements f as

$$f = |\mathcal{A}u + \epsilon|$$

where ϵ denotes the additive noise, and one readily sees that the noise happens to $\mathcal{A}u$. In summary, we aim to bridge the gap between the PR algorithm and the image processing methods in this paper. The core idea in this paper is quite close to the error reduction algorithm [16] for PR, and the alternating projection is computed between the magnitude constraint set and the sparsity promoted evolution.

III. Numerical algorithm and convergence analysis

In this section we will present the algorithm details in the following two subsections for the generalized least quare problem in the step 1 of (9) and the denoising problems in the Step 3 of (9) separately.

A. Step 1 of (9): Solving the generalized least square subproblems

We focus on solving the first subproblem this subsection. By setting $g = v^k - \frac{\Lambda^k}{r}$, it becomes

$$u^{k+1} = \mathrm{Prox}_{\mathbf{G}/r+I_{\mathscr{K}}}(g)$$

There are many choices for solve the traditional PR problems. However, these methods can not be directly applied to such model with additional quadratic term. An ADMM can be used directly to solve this problem. Similarly to [6], [45], we reformulate it by introducing $z = \mathcal{A}u$ as

$$\min_{u,z} \mathbf{B}(|z|^2, f) + I_{\mathscr{K}}(u) + \frac{r}{2}\|u-g\|^2, s.t. z = \mathcal{A}u, \quad (10)$$

with the corresponding augmented Lagrangian as

$$\hat{\mathcal{L}}_\eta(u,z;\hat{\Lambda}) = \mathbf{B}(|z|^2, f) + I_{\mathscr{K}}(u) + \frac{r}{2}\|u-g\|^2 + \mathrm{Re}(\langle z - \mathcal{A}u, \hat{\Lambda}\rangle) + \frac{\eta}{2}\|z-\mathcal{A}u\|^2.$$

The ADMM consists of three steps. For the subproblem with respect to the variable u, one shall compute the problem as

$$\min_{u\in\mathscr{K}} \frac{r}{2}\|u-g\|^2 + \frac{\eta}{2}\|\mathcal{A}u - (z+\hat{\Lambda}/\eta)\|^2.$$

If the constrained set $K = \mathbb{C}^n$, similarly to [46], the real and complex parts of minimizer of the above problem satisfies the the following equations

$$\begin{bmatrix} \eta\mathrm{Re}(\mathcal{A}^*\mathcal{A}) + r\mathbf{I} & -\mathrm{Im}(\mathcal{A}^*\mathcal{A}) \\ \mathrm{Im}(\mathcal{A}^*\mathcal{A}) & \eta\mathrm{Re}(\mathcal{A}^*\mathcal{A}) + r\mathbf{I} \end{bmatrix} \begin{bmatrix} \mathrm{Re}(u) \\ \mathrm{Im}(u) \end{bmatrix} = \begin{bmatrix} \eta\mathrm{Re}(\mathcal{A}^*\hat{z}) + r\mathrm{Re}(g) \\ \eta\mathrm{Im}(\mathcal{A}^*\hat{z}) + r\mathrm{Im}(g) \end{bmatrix}, \quad (11)$$

with $\hat{z} = z + \hat{\Lambda}/\eta$.

We can simplify the solution of above subproblem if the matrix $\mathcal{A}$ involves Fourier measurements with masks $\{I_k\}_{k=1}^K$ for coded diffraction pattern as

$$\mathcal{A}u = \begin{bmatrix} \mathcal{F}(w_0 \circ u) \\ \mathcal{F}(w_1 \circ u) \\ \vdots \\ \mathcal{F}(w_{K-1} \circ u) \end{bmatrix}, \quad (12)$$

where $\circ$ denotes the pointwise multiplication, w_k is a (mask) matrix indexed by k, each of which is represented by a vector in $\mathbb{C}^n$ in a lexicographical order. Therefore we have $\mathcal{A}^*\mathcal{A} = \sum_j w_j^* \circ w_j$, which is a real-valued matrix. Finally we have

$$u_{min} = \big(\eta\mathcal{A}^*\mathcal{A} + r\mathbf{I}\big)^{-1}\big(\eta\mathcal{A}^*(z+\hat{\Lambda}/\eta) + rg\big), \quad (13)$$

since the diagonal matrix $\eta\mathcal{A}^*\mathcal{A} + r\mathbf{I}$ is non-singular. One can easily get the same equations as (13) for ptychographic PR, and we omit the details here. However, if $\mathscr{K} \neq \mathbb{C}^n$, it requires us to introduce additional variable to establish the ADMM as [45]. In order to simplify the algorithm, one can use an additional projection step for such case.

For the subproblem with respect to the variable z, the following subproblem should be considered

$$\min_z \mathbf{B}(|z|^2, f) + \frac{\eta}{2}\|z - z_0\|^2,$$

with $z_0 := \mathcal{A}u - \hat{\Lambda}/\eta$.

When the measurement is contaminated by the Poisson noise, we can directly get the solution to the minimization problem

$$\min_z \frac{1}{2}\langle |z|^2 - 2f\log|z|, \mathbf{1}\rangle + \frac{\eta}{2}\|z - z_0\|^2, \tag{14}$$

following [70], [46] in the following lemma.

Lemma III.1. *The minimizer to* (14) *is*

$$z_{min}(j) = \frac{\eta|z_0(j)| + \sqrt{\eta^2|z_0(j)|^2 + 4(1+\eta)f(j)}}{2(1+\eta)} \times \mathrm{sign}(z_0(j)), \tag{15}$$

for all $j \in \tilde{\Omega}$.

When the noise is Gaussian, a direct L^2 data fitting term can be obtained by the MAP as the first equation in (4). Hence the minimization problem should be considered as

$$\min_z \frac{1}{2}\big\||z|^2 - f\big\|^2 + \frac{\eta}{2}\|z - z_0\|^2. \tag{16}$$

We give a lemma to show how to compute such problem.

Lemma III.2. *The minimizer to* (16) *is*

$$z_{min}(j) = \rho(j)\mathrm{sign}(z_0(j)), \tag{17}$$

where $\mathrm{sign}(z_0(j)) = \dfrac{z_0(j)}{|z_0(j)|}$, *and*

$$\rho(j) = \begin{cases} \sqrt[3]{\dfrac{\eta|z_0(j)|}{4} + \sqrt{D(j)}} + \sqrt[3]{\dfrac{\eta|z_0(j)|}{4} - \sqrt{D(j)}}, & \text{if } D(j) \geq 0; \\ 2\sqrt{(f(j) - \eta/2)/3}\cos\big(\arccos(\theta_j/3)\big), & \text{otherwise,} \end{cases} \tag{18}$$

for all $j \in \tilde{\Omega}$, *with*

$$D(j) = \frac{(\eta/2 - f(j))^3}{27} + \frac{\eta^2|z_0(j)|^2}{16},$$

and

$$\theta(j) = \frac{\eta|z_0(j)|}{4\sqrt{-(\eta/2 - f(j))^3/27}}.$$

Proof. One readily sees that the optimization procedure is independent for each entry of z. Therefore we only consider the problem for each entry $z(i)$ as

$$z_{min}(j) = \arg\min_{z(j)} \frac{1}{2}\big||z(j)|^2 - f(j)\big|^2 + \frac{\eta}{2}|z(j) - z_0(j)|^2.$$

Then we have $z_{min}(j) = \rho(j)\mathrm{sign}(z_0(j))$, where $\rho(j) \geq 0$. We focus on the determination of $\rho(j)$ as

$$\rho(j) = \arg\min_{x \geq 0} \phi(x), \tag{19}$$

with

$$\phi(x) := \frac{1}{2}(x^2 - f(j))^2 + \frac{\eta}{2}(x - |z_0(j)|)^2.$$

The stationary points of the above problem satisfy the following cubic equation as

$$x^3 + \big(-f(j) + \frac{\eta}{2}\big)x - \frac{\eta}{2}|z_0(j)| = 0.$$

The minimizer should be either the stationary points of $\phi(x)$ or zero. Based on a simple discussion by Vieta's formulas and the close solution to cubic equation [71], it only has one real non-negative root as (18), which is also the unique minimizer of (19). Therefore, we can compute the value the non-negative root $\rho(j)$ by (17) to get the minimizer of (19), that concludes to this lemma. □

In summary, we give the overall algorithm for this subproblem of Step 1 in (9) as

$$\begin{cases} \text{Step 1: Solve } u_{k+1} \text{ by (11) with } (z, \hat{\Lambda}) := (z_k, \hat{\Lambda}_k), \\ \text{Step 2: Solve } z_{k+1} \text{ by (17) and (15)} \\ \qquad\qquad \text{with } (u, \hat{\Lambda}) := (u_{k+1}, \hat{\Lambda}_k), \\ \text{step 3: Update } \ \hat{\Lambda}_{k+1} \text{ as} \\ \qquad\qquad \hat{\Lambda}_{k+1} = \hat{\Lambda}_k + \eta(z_{k+1} - \mathcal{A}u_{k+1}), \end{cases} \tag{20}$$

for the $(k+1)^{th}$ iterations if provided with $(u_k, z_k, \hat{\Lambda}_k)$.

B. Step 3 of (9)*: Denoising subproblems with respect to the variable* v

As mentioned above, two kinds of operators can be considered. First one is the variational image methods as ROF, LLT, NLTV and TGV, and the other kind is the filter such as the bilateral filter, nonlocal means filter and BM3D filter.

1) Variational methods: One needs to compute the subproblem of the third step of (9) as

$$\min_{v \in \mathbb{C}^n} \sigma\mathbf{R}(v) + \frac{1}{2}\|v - v_0\|^2, \tag{21}$$

where we rewrite (8) with $v_0 := v^k - \frac{\Lambda^k}{r}$.

First for the underling real-valued image, one can directly use the existing algorithm to solve the variational models. However, in order to deal with the complex-valued image, we should give precise definition of TV as

$$\mathrm{TV}(v) = \sqrt{\sum_j |(\mathrm{D}_x v)_j|^2 + |(\mathrm{D}_y v)_j|^2},$$

where $\mathrm{D}_x(\cdot), \mathrm{D}_y(\cdot)$ denote the forward difference operators of the complex-valued image with respect to the x-direction and y-direction. For TV based denoising, we need to compute the minimization problem (8) as

$$\min_{v \in \mathbb{C}^n} \sigma\mathrm{TV}(v) + \frac{1}{2}\|v - v_0\|^2,$$

with the complex-valued variable v_0. By introducing the variable $p = \nabla u := (\mathrm{D}_x u, \mathrm{D}_y u)$, we have to solve the following saddle point problem as

$$\max_{\Psi}\min_{p,v} \quad \sigma\|p\| + \frac{1}{2}\|v - v_0\|^2 + \mathrm{Re}(\langle p - \nabla v, \Psi\rangle) + \frac{\gamma}{2}\|p - \nabla v\|^2,$$

with a positive constant γ. It consists of three steps w.r.t the variables v, p and the update of the multiplier Ψ. For the subproblem w.r.t v, one needs to solve

$$\min_v \frac{1}{2}\|v - v_0\|^2 + \frac{\gamma}{2}\|p + \frac{1}{\gamma}\Psi - \nabla v\|^2.$$

The above minimization problem can be considered as minimizing of the real and the complex parts of the variable v independently, and therefore by simply separating the real and complex parts of v as (11) and computing the stationary points, we have

$$\begin{cases} (-\gamma\Delta + \mathbf{I})\mathrm{Re}(v) = \mathrm{Re}(v_0) + \gamma\mathrm{Re}(\nabla(p - \frac{1}{\gamma}\Psi)), \\ (-\gamma\Delta + \mathbf{I})\mathrm{Im}(v) = \mathrm{Im}(v_0) + \gamma\mathrm{Im}(\nabla(p - \frac{1}{\gamma}\Psi)), \end{cases}$$

where $\Delta u = \nabla \cdot \nabla u$, $\nabla \cdot p$ denotes the backward difference operator of p which satisfies the adjoint relation as

$$\langle \nabla v, p\rangle = -\langle v, \nabla \cdot p\rangle.$$

Finally we obtain the uniform formula for the complex-valued image as

$$(-\gamma\Delta + \mathbf{I})(v) = v_0 + \gamma\nabla(p - \frac{1}{\gamma}\Psi), \tag{22}$$

which actually has a same form for the real-valued image. Furthermore, if using the periodical boundary condition for variable v, fast Fourier transformations (FFTs) can be used to solve the above problem with optimal time complexity.

For the subproblem w.r.t the variable p, one needs to compute the minimizer p_{min} by the soft thresholding as

$$p_{min} = \max\{0, |\nabla v - \Psi/r| - \sigma/\gamma\} \circ \mathrm{sign}(\nabla v - \Psi/r). \tag{23}$$

In summary, combining the solutions v_{k+1} of (22) and the solution p_{k+1} of (22) with the update of the multipliers Ψ by

$$\Psi_{k+1} = \Psi_k + \gamma(p_{k+1} - \nabla v_{k+1}),$$

a fast minimization algorithm for the subproblem (8) is established. For other kind of higher order TV models, one can readily build the efficient ADMMs just by considering the complex-valued image instead of the real-valued image, since the analysis of solving the above TV model demonstrates the similarity of the cases between the real-valued and complex-valued image. Limited to the space, we do not give all the detailed algorithms for them.

2) Filters based methods: There are a considerable mount of filters for image denoising, and a very comprehensive and deep review was given in [72], where it showed that the bilateral filter, boosting, kernel, and spectral method, and nonlocal means and so on are deeply connected with the current popular iterative methods as the Bregman iterations [73]. Among these filters, we focus on NLM and BM3D filters in this paper, which promote the patch sparsity and can be used for the complex-valued image directly.

The nonlocal mean filter can be defined as a linear combination of the nonlocal neighbours [66] as

$$\mathrm{NLM}(v)(x) = \sum_{y\in\Omega_x} w(x,y)v(y), \ \forall x \in \Omega,$$

where v is the noisy image, the nonlocal weight function $w(x,y)$ measures the similarity between two pixels satisfying $w(x,y) \geq 0, \ \sum_{y\in\Omega_x} w(x,y) = 1, \ \forall x \in \Omega, \ y \in \Omega_x$, and the region Ω_x is the search window at point x which is usually square and selected over the entire image. Nonlocal total variation regularized methods and fast algorithms stimulated by the nonlocal means were also developed [74], [64] for image deblurring, inpainting and reconstruction.

Different to the idea employing the weighted average of nonlocal patches from the noisy image, BM3D enhanced the sparsity by grouping 2D image patches consisting of similar structures or features into 3D patches. Four steps includes (1) Analysis step: Grouping the similar patches into a 3D blocks and linear transformation of the 3D blocks, (2) Processing: Hard thresholding of the transform domain, and (3) Synthesis: Inverse 3D transformation of the shrinkage of the transform domain to the image domain. The variational methods combining the BM3D filter for image deblurring were proposed in [61] and inpainting [52], [68] based on the regularization by L^p norm of the transform domain. The Nash equilibrium problem as a bilevel optimization problem was further presented, and therefore the method by a direct use of BM3D filter greatly improved the restoration results of traditional variational methods with the single-objective minimization problem.

C. Theoretical analysis

We will give the theoretical analysis of the proposed framework in (9). The denoising subproblem is well defined for both the regularized term or the filters. First we analyze the convergence of ADMM for the generalized least square subproblem in (20). Readily one can infer that the functional $\mathbf{G}(u)$ is nonconvex, which leads to the main challenge for the convergence study. However, from the numerical performances, it is quite robust. Following [6], we give the convergence results as follows.

Proposition III.1. *Assuming that the multiplier of* (10) *exists, the sequences of the multipliers* $\hat{\Lambda}_{k+1} - \hat{\Lambda}_k \to 0$ *as* $k \to \infty$, *and* $\{u_k\}$ *is bounded, then there exists an accumulative point of* $\{u_k, z_k, \hat{\Lambda}_k\}$ *satisfies the Karush-Kuhn-Tucker (KKT) condition of* (10) *(a stationary point).*

Proof. See the detailed proof in the Refs. [6], [45], [46]. □

Here we give a very general assumption of the convex regularization $\mathbf{R}(v)$ as follows.

Assumption III.1. *The functional* $\mathbf{R}(v)$ *is proper, closed, and convex, and lower semi-continuous.*

We analyze the convergence of the ADMM for the denosing step of (9) when variational regularization models are incorporated in.

Proposition III.2. *The ADMM converges to the unique global minimizer of* (21) *for the denoising step of* (9).

Proof. Readily one can prove the unique existence of the minimizer to (21) under Assumption III.1. By lifting the

dimension of the complex-valued variable v by separating the corresponding complex and real parts as [46], one can conclude this proposition for this convex minimization problem following [49], [50]. □

We have shown the convergence study of the algorithms for each subproblems, and one can also derive the following convergence theorem for the general framework in (9) if the convex variational regularization functional $\mathbf{R}(v)$ satisfies Assumption III.1.

Theorem 1. *If the subproblems in Step 1 and Step 3 are exactly solved, the algorithm in* (9) *is convergent, i.e. the iterative sequences have an accumulative point* (u^*, v^*, Λ^*)*, which satisfies the KKT condition of* (6) *if the sequences* $\{\Lambda^{k+1} - \Lambda^{k+1/2}\}$ *or* $\{\Lambda^{k+1/2} - \Lambda^k\}$ *converge to zero and* $\{u^k\}$ *is bounded.*

Proof. One needs to prove (u^*, v^*, Λ^*) satisfies that

$$\begin{cases} 0 \in \nabla_u \mathbf{G}(u^*) + \partial_u I_{\mathscr{K}}(u^*) + \Lambda^*, \\ 0 \in \lambda \partial_v \mathbf{R}(v^*) - \Lambda^*, \\ 0 = u^* - v^*. \end{cases} \tag{24}$$

We finish the proof in two steps. In Step 1, we prove the boundedness of the iterative solutions. First by the multiplier update steps, the sequence $\{v^k\}$ is bounded as a result of the boundedness of $\{u^k\}$. Therefore, the multiplier $\{\Lambda^{k+1/2}\}$ is bounded due to $(u^{k+1} + \Lambda^{k+1/2}/r) - v^{k+1} \in \frac{\lambda}{r}\partial_v \mathbf{R}(v^{k+1})$. With the assumption of the convergence of $\{\Lambda^{k+1} - \Lambda^{k+1/2}\}$ or $\{\Lambda^{k+1/2} - \Lambda^k\}$, the boundedness of $\{\Lambda^k\}$ is derived. Therefore there exists a subsequence $\{u^k, v^k, \Lambda^k\}$ (still use the same notation to represent this subsequence) and a triple (u^*, v^*, Λ^*), such that

$$\{u^k, v^k, \Lambda^k\} \to \{u^*, v^*, \Lambda^*\} \text{ as } k \to \infty.$$

In Step 2, we will prove the triple (u^*, v^*, Λ^*) satisfies (24). One can readily has $u^* = v^*$ by taking limit in the step of multiplier updates. Readily one has

$$\begin{aligned} &\mathbf{G}(u^{k+1}) + I_{\mathscr{K}}(u^{k+1}) + \frac{r}{2}\|u^{k+1} - (v^k - \Lambda^k/r)\|^2 \\ &- \frac{r}{2}\|u - (v^k - \Lambda^k/r)\|^2 \leq \mathbf{G}(u) + I_{\mathscr{K}}(u) \ \forall \ u \end{aligned}$$

By taking limits of u^k, v^k, Λ^k, and the lower semi-continuity of $\mathcal{G}$ and $I_{\mathscr{K}}$, one has

$$\begin{aligned} &\mathbf{G}(u^*) + I_{\mathscr{K}}(u^*) + \frac{r}{2}\|u^* - (v^* - \Lambda^*/r)\|^2 \\ \leq &\mathbf{G}(u) + I_{\mathscr{K}}(u) + \frac{r}{2}\|u - (v^* - \Lambda^*/r)\|^2 \ \forall \ u, \end{aligned}$$

which is the first relation of the KKT condition. The second one can be derived in a similar manner. That concludes to the theorem. □

The convergence of the proposed method combining the filters is much difficult than the above case, since one does not know the explicit form of $\mathbf{R}(v)$ for a general filters such as NLM and BM3D. The convergence is only limited to the fixed-point sense. We give the following assumption.

Assumption III.2. *There exists a fixed point* (u^*, v^*, Λ^*) *for the framework* (9)*, i.e.*

$$\begin{cases} u^* = \mathrm{Prox}_{\mathbf{G}/r + I_{\mathscr{K}}}(v^* - \Lambda^*/r), \\ v^* = \mathbf{D}_\sigma(u^* + \Lambda^*/r), \\ u^* = v^*, \end{cases} \tag{25}$$

where

$$\mathrm{D}_\sigma(u) := \mathrm{Prox}_{\sigma \mathbf{R}}(u)$$

represents a filter.

We can eliminate v^* in order to get the following form for (u^*, Λ^*)

$$\begin{cases} u^* = \arg\min_u \mathrm{Prox}_{\mathbf{G}/r + I_{\mathscr{K}}}(u^* - \Lambda^*/r), \\ u^* = \mathbf{D}_\sigma(u^* + \Lambda^*/r). \end{cases} \tag{26}$$

Using the condition as Theorem 1, we have the following theorem as follows.

Theorem 2. *Assume the filter is continuous, i.e.*

$$\mathbf{D}_\sigma(\hat{v}_k) \to \mathbf{D}_\sigma(\hat{v}^*) \text{ if } \hat{v}_k \to \hat{v}^* \text{as } k \to \infty.$$

If the subproblem in Step 1 are exactly solved, the algorithm in (9) *is convergent, i.e. the iterative sequences have an accumulative point* (u^*, v^*, Λ^*)*, which is a fixed point of* (25) *if the sequences* $\{\Lambda^{k+1} - \Lambda^{k+1/2}\}$ *or* $\{\Lambda^{k+1/2} - \Lambda^k\}$ *converge to zero and* $\{u^k\}$ *is bounded.*

Proof. It can be readily proved similarly to the proof of Theorem 1, and we omit the details here. □

Remark III.1. *In the above theorem, we assume that the filter operator is continuous. In real applications, the operator possibly relies on the image and therefore one can hardly give a verification. In the work [75], the operator is assumed to be bounded, and their proposed method with adaptive steps is convergent to its fixed point if* $\mathrm{R}(v)$ *has bounded gradient, that can not apply to the data fitting term in our model.*

IV. Experiments and discussion

A. Numerical implementation

In the numerical part, we set $\mathscr{K} = \mathbb{R}^n$ and $\mathbb{C}^n$ for real-valued and complex-valued image respectively in (1). Although we have given a framework for PR with arbitrary linear operator $\mathcal{A}$, we only show the performance on Fourier measurements involved with two types of patterns of linear operators $\mathcal{A}$: coded diffraction pattern (CDP) with random masks and ptychographic PR with zone plate lens. For the first pattern, the octanary CDP is explored, and specifically each element of I_j in (12) takes a value randomly among the eight candidates, *i.e.*, $\{\pm\sqrt{2}/2, \pm\sqrt{2}\mathbf{i}/2, \pm\sqrt{3}, \pm\sqrt{3}\mathbf{i}\}$. Set $K = 2, 4$ for real-valued and complex-valued image respectively as [46]. The setting of ptychographic PR is given as follows. The number of frames is 16×16 with sliding distance 16 pixels and the frame size 64×64. The len and the generated illumination are shown in Figure 1.

The ground truth images consist of five images including four real-valued with 512×512 pixels and one complex-valued with 256×256 pixels.

(a) (b)

Fig. 1. Lens in (a) and the generated illumination in (b) used for ptychographic PR.

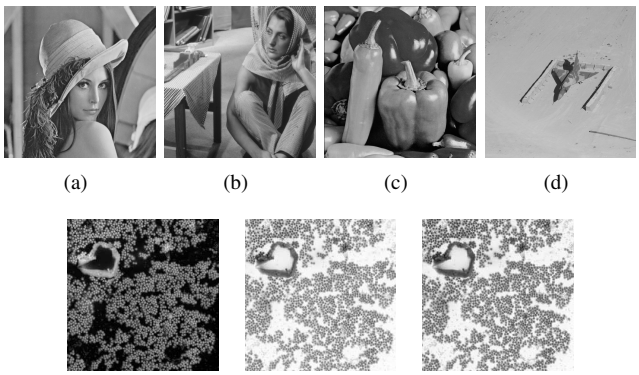

(a) (b) (c) (d)

(e) (f) (g)

Fig. 2. Ground truth images. Real-valued images (512×512 pixels) "Lena" in (a), "Barbara" in (b), "Peppers" in (c), "Plane" in (d), and complex valued image (256×256 pixels) with magnitude in (e), real and imaginary parts in (f) and (g) respectively.

The Poisson noise is added to the clean image with different peak levels, and different scale image u_ν are used as $u_\nu = \nu u$ with the peak level ν for ground truth u. We measure the quality of the reconstructed the image $\tilde{u}$ by

$$\mathrm{SNR}(\tilde{u}, u) = -20 \log(\|c^* \tilde{u} - u\| / \|c^* \tilde{u}\|),$$

with the ground truth image u, and a scale constant as

$$c^* = \max_{|c|=1} \|c\tilde{u} - u\|.$$

For Gaussian noise, SNR is also used to measure the noise level for the contaminated data.

There are many choices for PR without regularization, such as error reduction (ER)[16], ADMM [6], [45], [46], Wirtinger flow [28], [29] and so on, while we only use the ADMM for comparison. For the methods with regularization, we compare with TV based method in [46] for Poisson noise, and a variant method by inserting (17) for Gaussian noise. For our proposed methods, the second order TGV realization of $\mathbf{R}(v)$ and two filters including NLM, and BM3D are used. For simplicity, we use "LS-PR" to denotes the ADMM for solving the original PR problem without any regularization, "TV-PR" for TV based methods in [46], "TGV-PR" for our proposed method with TGV regularization, "NLM-PR" for our proposed method with NLM filtering, and "BM3D-PR" with BM3D filtering. It is quite difficult to set a unify fair stopping condition for such different algorithms, and the algorithms are all stopped if they reach a maximum iteration number T, where T is select heuristically. For "LS-PR" and "TV-PR", set $T = 50$, while for "TGV-PR", "NLM-PR" and "BM3D-PR", set $T = 30$ (the iterations number are more than real number needed, and usually $10 \sim 15$ iterations are sufficient to produce satisfactory results). In the inner loop for solving the generalized least square problem, five inner iterations are adopted. The other parameters used in the experiments will be addressed in the following subsections.

All the tests are performed on a laptop with Intel i7-5600U2.6GHZ, and 16GB RAM. The implementation of the codes is in MATLAB. For our proposed methods, we solve the denoising subproblem with TGV with the package by S. Keiichiro [1], NLM filter by J.V. Manjón [2] and BM3D by K. Dabov [3].

B. Poisson noise removal

1) Coded diffraction pattern (CDP): For CDP, we first show the performance on real-valued images in (a)-(d) of Figure 2 with different noise levels by setting the peak level $\nu \in \{3.0 \times 10^{-3}, 5.0 \times 10^{-3}, 1.0 \times 10^{-2}\}$, and see the results in Figure 3-Figure 5. With a fixed noise level the parameters of each compared methods are set to the same for each image, and see the detailed parameters in Table I.

By observing the reconstructed images in Figure 3-Figure 5, if the noise is not so heavy, all the methods work well as shown in Figure 3. When noise level increases as in Figure 4, results by "LS-PR" show obvious noise, while all the regularized and filtering methods can work. If the noise level is very high as in Figure 5, the reconstructed results by "LS-PR" can not be acceptable, while "NLM-PR" and "BM3D-PR" outperforms the others. "TV-PR" with simple regularization by TV is effective to generate the noiseless images for different noise level, and meanwhile it introduces the staircase artifacts and break some important information as texture; "TGV-PR" can suppress the staircase artifacts, and produce resulted images with sharp edges. However, the repetitive structures can not be kept. It seems that "NLM-PR" and "BM3D-PR" can both deal with the texture parts well, e.g. the hair of "Lena" and the stripe structures of "Barbara", which outperform other compared methods. Meanwhile, it seems that "BM3D-PR" produces the cleanest background for "Plane" among all the compared methods. The SNRs are put in Figure 6, where one can readily see that our proposed "TGV-PR", "NLM-PR" and "BM3D-PR" outperform "TV-PR", and "BM3D-PR" gains the largest SNRs among them. The average SNRs are $6.10, 20.32, 20.87, 21.98, 22.94$ dB for "LS-PR", "TV-PR", "TGV-PR", "NLM-PR" and "BM3D-PR" respectively, and "BM3D-PR" improves the image quality with SNRs about 2dB higher than that of "TV-PR" on average.

Numerical experiments for CDP is also performed on the complex-valued image of Figure 2 (e), and we show the recovery results in Figure 7 with different noise level by setting the peak level $\nu \in \{5.0 \times 10^{-2}, 8.0 \times 10^{-2}, 1.0 \times 10^{-1}\}$. One can readily see that with high level noise as the first

[1] https://www.mathworks.com/matlabcentral/mlc-downloads/downloads/submissions/49717/versions/2/download/zip

[2] https://www.mathworks.com/matlabcentral/mlc-downloads/downloads/submissions/13176/versions/1/download/zip

[3] http://www.cs.tut.fi/~foi/GCF-BM3D/BM3D.zip

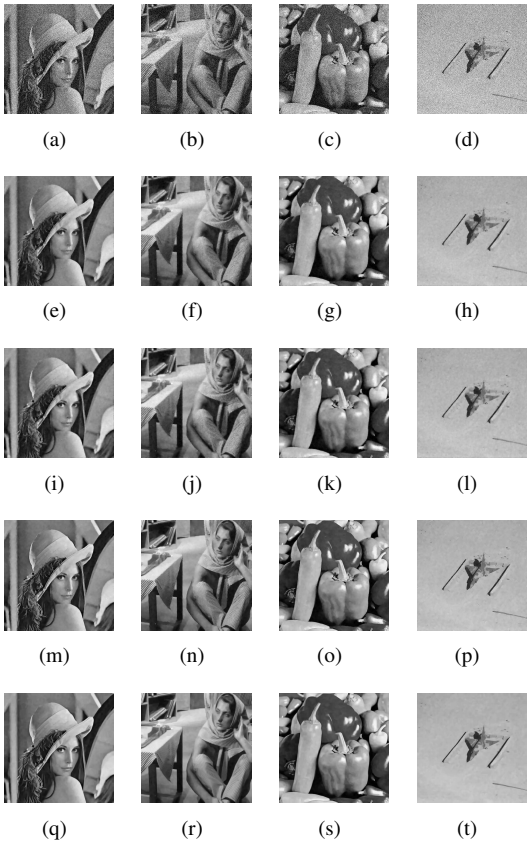

Fig. 3. PR with CDP. Peak level $\nu = 1.0 \times 10^{-2}$ for Poisson noise. First row: "LS-PR"; Second row: "TV-PR"; Third row: "TGV-PR"; Fourth row: "NLM-PR"; Fifth row: "BM3D-PR".

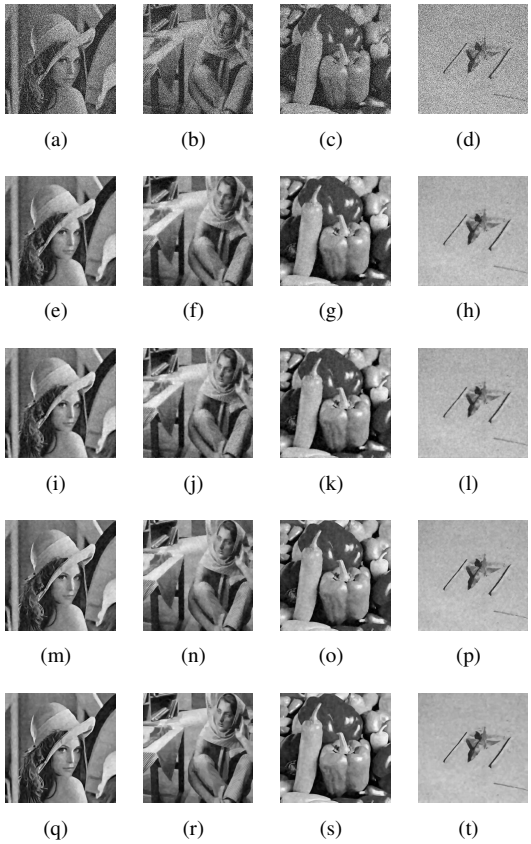

Fig. 4. PR with CDP. Peak level $\nu = 5.0 \times 10^{-3}$ for Poisson noise. First row: "LS-PR"; Second row: "TV-PR"; Third row: "TGV-PR"; Fourth row: "NLM-PR"; Fifth row: "BM3D-PR".

Method	Peak level ν	λ	r	η
TGV-PR	3.0×10^{-3}	7.0×10^{2}	5.0×10^{5}	50
	5.0×10^{-3}	6.0×10^{2}		
	1.0×10^{-2}	5.0×10^{2}		
NLM-PR	3.0×10^{-3}	6.0×10^{4}	1.0×10^{6}	
	5.0×10^{-3}	5.0×10^{4}		
	1.0×10^{-2}	3.0×10^{4}		
BM3D-PR	3.0×10^{-3}	1.5×10^{5}	5.0×10^{5}	
	5.0×10^{-3}	2.0×10^{5}		
	1.0×10^{-2}	2.0×10^{5}		

TABLE I
PARAMETERS FOR POISSON NOISE REMOVAL OF CDP ON REAL-VALUED IMAGES FOR FIGURE 3-FIGURE 5.

Method	Peak level ν	λ	r	η
TGV-PR	5.0×10^{-2}	2	5.0×10^{5}	100
	8.0×10^{-2}			
	1.0×10^{-1}			
NLM-PR	5.0×10^{-2}	4.0×10^{4}	1.0×10^{6}	50
	8.0×10^{-2}	3.5×10^{4}		
	1.0×10^{-1}	3.5×10^{4}		
BM3D-PR	5.0×10^{-2}	8×10^{4}	4.0×10^{5}	
	8.0×10^{-2}	1.5×10^{5}	1.0×10^{6}	
	1.0×10^{-1}	1.5×10^{5}	1.0×10^{6}	

TABLE II
PARAMETERS FOR POISSON NOISE REMOVAL OF CDP ON COMPLEX-VALUED IMAGES FOR FIGURE 7.

column of Figure 7, "TV-PR", and our proposed methods can remove the noise in the background. However, "TV-PR" and "TGV-PR" can not preserve the small structure at all. It seems that "NLM-PR" learns the wrong feature patterns. Parameters used are put in Table II. "BM3D-PR" is the most effective, which not only obtain clean background, but also recover some smaller structures. When the noise level decreases, "NLM-PR" still fails to find correct patterns for smaller structures, while the other methods can preserve both the larger and smaller scales features. We put the SNRs in Figure 8, and one can observe the increase of SNRs by our proposed methods. The average SNRs are 2.64, 10.15, 11.78, 10.50 and 12.76 for all the five methods, and "BM3D-PR" improves the reconstructed images with highest SNRs among them, and about 2.5dB is increased compared with those by "TV-PR" even for such complicated image. Moreover, the SNR increase of "BM3D-PR" comparing with those of "LS-PR" and "TV-PR" is the biggest among the four different images in Figure 8, which implies that it is quite suitable for the images with textures.

2) Ptychographic PR (Ptycho-PR): The complex-valued image in Figure 2 (e) are tested to show the performance of our proposed methods with different noise level by setting

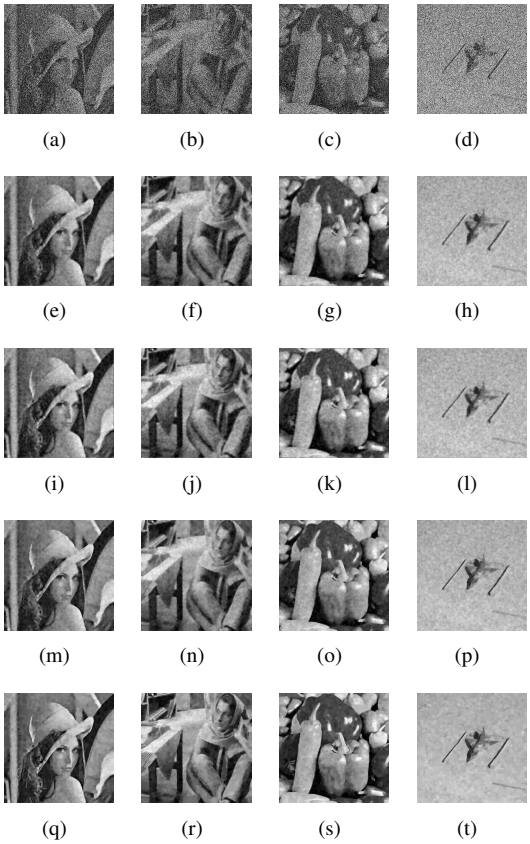

Fig. 5. PR with CDP. Peak level $\nu = 3.0 \times 10^{-3}$ for Poisson noise. First row: "LS-PR"; Second row: "TV-PR"; Third row: "TGV-PR"; Fourth row: "NLM-PR"; Fifth row: "BM3D-PR".

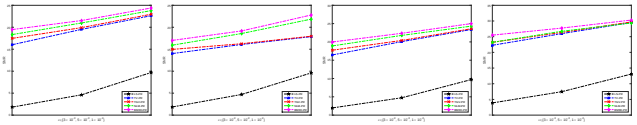

(a) "Lena" (b) "Barbara" (c) "Peppers" (d) "Plane"

Fig. 6. SNRs for images in Figure 7 v.s. different peak levels ν by the methods with CDP.

the peak level $\nu \in \{0.2, 0.5, 0.8\}$, and see results in 9 and SNRs in Figure 10, where we only show the performances of "LS-PR","TV-PR" and "BM3D-PR". We fix the parameters as $\lambda = 7.0 \times 10^3, r = 7.0 \times 10^4$ and $\eta = 5$ for different noise levels. Reconstructed images are blurry by "LS-PR", which seems more challengeable than CDP with random masks. With high level noise, "TV-PR" recovers the images with sharp edges and clean background, but almost completely blurs the smaller scale features. "BM3D-PR" can work well and some of the features are recovered when one can hardly see any smaller features from the images by "LS-PR". When the noise level decreases, "TV-PR" and "BM3D-PR" can work well. Again "BM3D-PR" gains the highest SNRs inferred from Figure 12. The average SNRs are 8.60, 13.67, and 15.89 for "LS-PR", "TV-PR", and "BM3D-PR" respectively, and our proposed method has about 2dB increase averagely compared with "TV-PR".

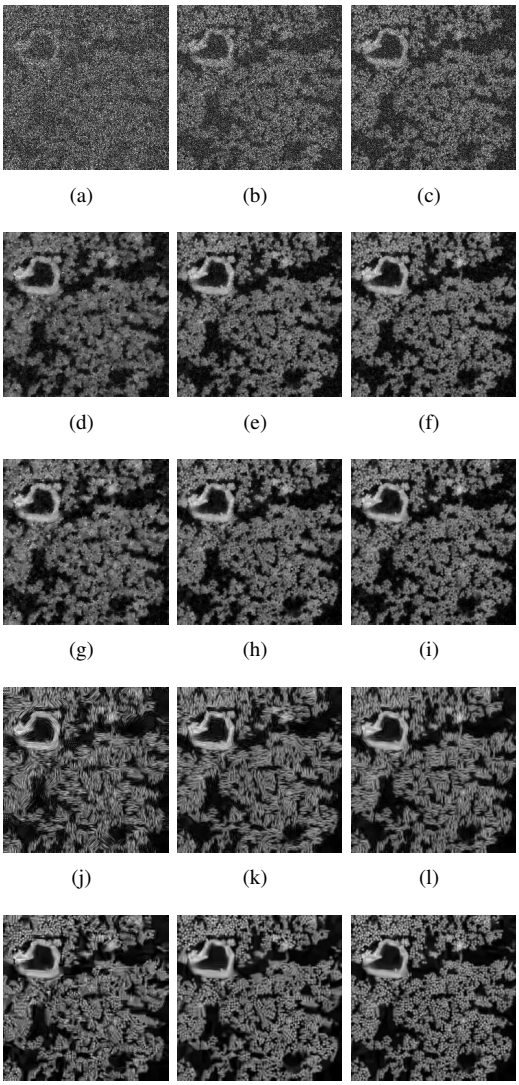

Fig. 7. PR with CDP. Peak level $\nu = 5.0\times10^{-2}, 8.0\times10^{-2}, 1.0\times10^{-1}$ for Poisson noise from left to right. First row: "LS-PR"; Second row: "TV-PR"; Third row: "TGV-PR"; Fourth row: "NLM-PR"; Fifth row: "BM3D-PR".

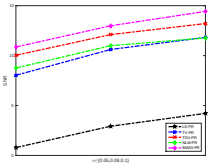

(a)

Fig. 8. SNRs for reconstructed images in Figure 7 v.s. peak level ν for different methods with CDP.

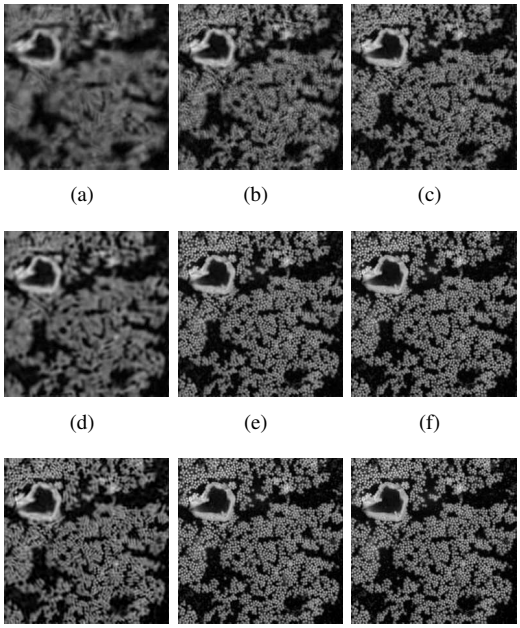

(a) (b) (c)

(d) (e) (f)

(g) (h) (i)

Fig. 9. Ptychographic PR. Peak level $\nu = 0.2, 0.5, 0.8$ for Poisson noise from left to right. First row: "LS-PR"; Second row: "TV-PR"; Third row: "BM3D-PR".

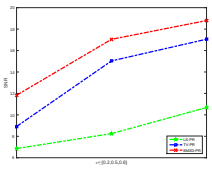

(a)

Fig. 10. SNRs of the reconstructed images in Figure 9 v.s. peak level ν by different methods for ptychographic PR.

C. Gaussian noise

We only consider the ptychographic PR in this part, and see the results in Figure 11. Set parameters of "BM3D-PR" as $\lambda = 3.5\times10^7, 1.5\times10^7, 1.0\times10^7$ for the noisy measurements with SNRs to be 15, 20, and 30 respectively. Fix the parameter $r = 2.5\times10^7$, and $\eta = 1.0\times10^3$ with different noise levels. The reconstructed images by "LS-PR" only keep the large-scale features, and completely lose the smaller ones. TV-PR just smooths the images, while also loses most of the smaller scale structures in Figure 11 (d) and (e). With our proposed "BM3D-PR", it can recover almost all of the texture parts in Figure 11 (h), and even contaminated by very severe noise, some of the smaller scale features can be preserved in Figure 11 (g). The SNRs are put in Figure 12, and one can readily observe the increase of the SNRs by our method. The average SNRs are 6.41, 9.65, and 11.09 for "LS-PR", "TV-PR" and "BM3D-PR" respectively, and our method gains about 3dB, 1.5dB increase averagely compared with "LS-PR' and "TV-PR" respectively.

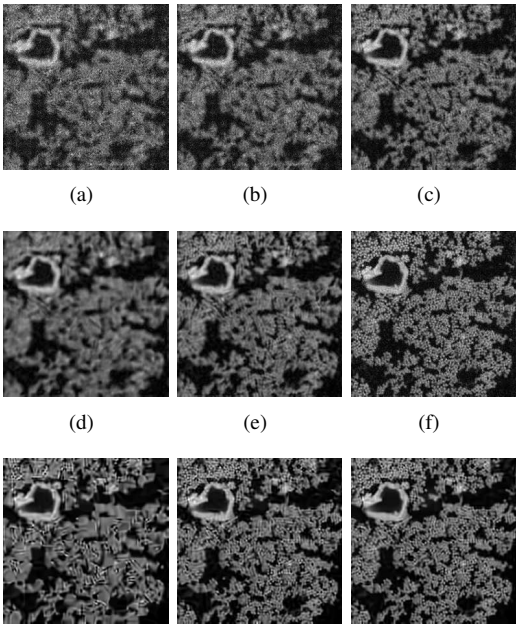

(a) (b) (c)

(d) (e) (f)

(g) (h) (i)

Fig. 11. Ptychographic PR. Noisy level of measurements with $\mathrm{SNR} = 15, 20, 30$ for Gaussian noise from left to right. First row: "LS-PR"; Second row: "TV-PR"; Third row: "BM3D-PR".

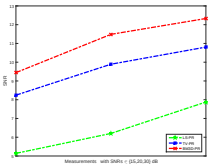

Fig. 12. SNRs for reconstructed images in Figure 11 v.s. measurements with $\mathrm{SNR} = 15, 20, 30$ for ptychographic PR.

D. Convergence

To check the convergence of the iteration process, we monitor the histories of SNRs and relative errors of iterative solution u^k w.r.t. the iteration number k, which are defined as $\frac{\|u^k - u^{k-1}\|}{\|u^k\|}$. We show the histories of errors and SNRs for CDP for our proposed "TGV-PR", "NLM-PR", and "BM3D-PR" on images "Lena" with Poisson noise, and see Figure 13 for detail. It demonstrates that our proposed methods are convergent and stable. For heavier noise, one needs more iterations to reach the final results with better image quality. Although we set the maximum iteration number as 30, about one third or half of the number is enough for real applications. It will be interesting to investigate how to set the optimal iteration number for different noise levels, and we put it as a future work.

We also perform an experiment to show the advantage of symmetric updating for our proposed methods compared with asymmetric style (remove Step 2 of (9)), and see the results in Figure 14 for the history of the SNRs. One can readily observe the acceleration by introducing the symmetric iteration. A possible direction is to adopt the adaptive step to updating the multipliers in order to further speedup the algorithm, and

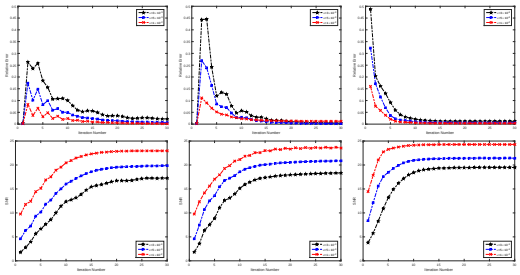

(a) TGV-PR (b) NLM-PR (c) BM3D-PR

Fig. 13. Convergence study by checking the histories of the SNRs and relative errors w.r.t. the iteration number. First row: The relative errors w.r.t. iteration number; Second row: The SNRs w.r.t. iteration number. From left to right: histories of relative errors and SNRs for "TGV-PR", "NLM-PR" and "BM3D-PR" respectively.

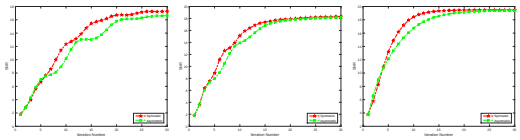

(a) TGV-PR (b) NLM-PR (c) BM3D-PR

Fig. 14. Performances comparison for symmetric updating and asymmetric updating. From left to right: histories of SNRs for "TGV-PR", "NLM-PR" and "BM3D-PR" respectively.

we also put it as a future work.

E. Stable performance for different parameters

Here the Poisson noise removal of CDP for real-valued image "Lena" is considered. Set peak level as $\nu = 3.0 \times 10^{-3}$. $\lambda^0 = 7.0 \times 10^2$, and $r^0 = 5.0 \times 10^5$ as shown in Table I. We test the performance of the proposed methods w.r.t the parameters λ and r, where we vary one with the other fixed. Particularly, we choose λ from $\{\lambda^0 \times 2^{-l}, \lambda^0 \times 2^{-l+1}, \cdots, \lambda^0 \times 2^{l-1}, \lambda^0 \times 2^l\}$ with $l = 5$ and fix $r = r^0$, and see the resulted SNRs in Figure 15 (a). The parameter λ play a role in balancing the data fitting term and regularization term. If the parameter λ becomes very small, regularization effect get relative weak, and as a result, the recovery results contain more noise. If it is very large, the recovery results go far away from the measurements, and one also recover the images with lower quality. Similarly, choose r from $\{r^0 \times 2^{-l}, r^0 \times 2^{-l+1}, \cdots, r^0 \times 2^{l-1}, r^0 \times 2^l\}$ with $l = 5$ and fixed $\lambda = \lambda^0$ and plot the corresponding SNRs of the reconstructed images in Figure 15 (b). Since the proposed methods solve the nonconvex optimization problem just simply by ADMM, it demonstrates we shall select a moderate value for parameter r.

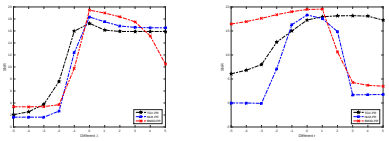

Fig. 15. Performances w.r.t. parameters λ and r.

V. Conclusion

In this paper, we propose a simple and flexible framework to retrieve phase from noisy measurements contaminated by Poisson or Gaussian nose. By incorporating higher order TV as TGV and nonlocal sparsity based filters as NLM and BM3D, the image are recovered with sharp edges, clean background and repetitive features. Numerical experiments show that even for the complicated complex-valued image with both large scale and repetitive smaller scale features, our proposed methods can work well compared with the traditional PR algorithm without regularization, and simple "TV-PR" method. Our proposed methods rely on some important parameters, and in the future it is very interesting to explore an automatical approach for selecting optimal parameters in practise.

Acknowledgment

Dr. H. Chang was partially supported by China Scholarship Council (CSC), National Natural Science Foundation of China (NSFC No. 11426165 and No. 11501413) and Tianjin 131 Talent Project. This work was also partially funded by the Center for Applied Mathematics for Energy Research Applications, a joint ASCR-BES funded project within the Office of Science, US Department of Energy, under contract number DOE-DE-AC03-76SF00098.

References

[1] A. Walther, "The question of phase retrieval in optics," *Journal of Modern Optics*, vol. 10, pp. 41–49, 1963.

[2] S. Marchesini, H. He, H. N. Chapman, S. P. Hau-Riege, A. Noy, M. R. Howells, U. Weierstall, and J. C. Spence, "X-ray image reconstruction from a diffraction pattern alone," *Physical Review B*, vol. 68, no. 14, p. 140101, 2003.

[3] R. W. Harrison, "Phase problem in crystallography," *J. Opt. Soc. Am. A*, vol. 10, no. 5, pp. 1046–1055, 1993.

[4] J. Miao, T. Ishikawa, Q. Shen, and T. Earnest, "Extending x-ray crystallography to allow the imaging of noncrystalline materials, cells, and single protein complexes," *Annu Rev Phys Chem.*, vol. 59, pp. 387–410, 2008.

[5] Y. Shechtman, Y. C. Eldar, O. Cohen, H. N. Chapman, J. Miao, and M. Segev, "Phase retrieval with application to optical imaging: a contemporary overview," *Signal Processing Magazine, IEEE*, vol. 32, no. 3, pp. 87–109, 2015.

[6] Z. Wen, C. Yang, X. Liu, and S. Marchesini, "Alternating direction methods for classical and ptychographic phase retrieval," *Inverse Probl.*, vol. 28, no. 11, p. 115010, 2012.

[7] I. Waldspurger, A. Aspremont, and S. Mallat, "Phase recovery, maxcut and complex semidefinite programming," *Math. Program., Ser. A*, pp. 1–35, DOI 10.1007/s10107-013-0738-9, 2012.

[8] K. Jaganathan, Y. C. Eldar, and B. Hassibi, "Phase retrieval: An overview of recent developments," *arXiv preprint arXiv:1510.07713*, 2015.

[9] D. Gabor *et al.*, "A new microscopic principle," *Nature*, vol. 161, no. 4098, pp. 777–778, 1948.

[10] J. t. Karle and H. Hauptman, "The phases and magnitudes of the structure factors," *Acta Crystallographica*, vol. 3, no. 3, pp. 181–187, 1950.

[11] D. Sayre, "The squaring method: a new method for phase determination," *Acta Crystallographica*, vol. 5, no. 1, pp. 60–65, 1952.

[12] M. Eckert, "Disputed discovery: the beginnings of x-ray diffraction in crystals in 1912 and its repercussions," *Acta Crystallographica Section A: Foundations of Crystallography*, vol. 68, no. 1, pp. 30–39, 2012.

[13] W. Hoppe, "Beugung im inhomogenen primärstrahlwellenfeld. i. prinzip einer phasenmessung von elektronenbeugungsinterferenzen," *Acta Crystallographica Section A: Crystal Physics, Diffraction, Theoretical and General Crystallography*, vol. 25, no. 4, pp. 495–501, 1969.

[14] J. Rodenburg and R. Bates, "The theory of super-resolution electron microscopy via wigner-distribution deconvolution," *Philosophical Transactions of the Royal Society of London A: Mathematical, Physical and Engineering Sciences*, vol. 339, no. 1655, pp. 521–553, 1992.

[15] H. N. Chapman, "Phase-retrieval x-ray microscopy by wigner-distribution deconvolution," *Ultramicroscopy*, vol. 66, no. 3, pp. 153–172, 1996.

[16] R. W. Gerchberg and W. O. Saxton, "A practical algorithm for the determination of the phase from image and diffraction plane pictures," *Optik*, vol. 35, no. 2, pp. 237–246, 1972.

[17] J. R. Fienup, "Phase retrieval algorithms: a comparison," *Appl. Opt.*, vol. 21, no. 15, pp. 2758–2769, 1982.

[18] H. H. Bauschke, P. L. Combettes, and D. R. Luke, "Phase retrieval, error reduction algorithm, and fienup variants: a view from convex optimization," *J. Opt. Soc. Amer. A*, vol. 19, no. 7, pp. 1334–1345, 2002.

[19] ——, "Hybrid projectioncreflection method for phase retrieval," *J. Opt. Soc. Amer. A*, vol. 20, no. 6, pp. 1025–1034, 2003.

[20] V. Elser, "Phase retrieval by iterated projections," *J. Opt. Soc. Am. A*, vol. 20, no. 1, pp. 40–55, 2003.

[21] D. R. Luke, "Relaxed averaged alternating reflections for diffraction imaging," *Inverse Probl.*, vol. 21, no. 1, pp. 37–50, 2005.

[22] S. Marchesini, "A unified evaluation of iterative projection algorithms for phase retrieval," *Review of scientific instruments*, vol. 78, no. 1, p. 011301, 2007.

[23] P. Netrapalli, P. Jain, and S. Sanghavi, "Phase retrieval using alternating minimization," *Signal Processing, IEEE Transactions on*, vol. 63, no. 18, pp. 4814–4826, 2015.

[24] S. Marchesini, Y.-C. Tu, and H.-T. Wu, "Alternating projection, ptychographic imaging and phase synchronization," *Applied and Computational Harmonic Analysis*, 2015.

[25] J. Qian, C. Yang, A. Schirotzek, F. Maia, and S. Marchesini, "Efficient algorithms for ptychographic phase retrieval," *Inverse Problems and Applications, Contemp. Math*, vol. 615, pp. 261–280, 2014.

[26] J. Zhong, L. Tian, P. Varma, and L. Waller, "Nonlinear optimization algorithm for partially coherent phase retrieval and source recovery."

[27] C. MA, X. LIU, and Z. WEN, "Globally convergent levenberg-marquardt method for phase retrieval," *preprint*.

[28] E. J. Candes, X. Li, and M. Soltanolkotabi, "Phase retrieval via wirtinger flow: Theory and algorithms," *IEEE Trans. Inf. Theory*, vol. 61, no. 4, pp. 1985–2007, 2015.

[29] Y. Chen and E. J. Candes, "Solving random quadratic systems of equations is nearly as easy as solving linear systems," *arXiv preprint arXiv:1505.05114*, 2015.

[30] P. Chen and A. Fannjiang, "Fourier phase retrieval with a single mask by douglas-rachford algorithm," *arXiv preprint arXiv:1509.00888*, 2015.

[31] E. J. Candes, T. Strohmer, and V. Voroninski, "Phaselift: Exact and stable signal recovery from magnitude measurements via convex programming," *Commu. Pure Applied Math.*, vol. 66, no. 8, pp. 1241–1274, 2013.

[32] R. Horstmeyer, R. Y. Chen, X. Ou, B. Ames, J. A. Tropp, and C. Yang, "Solving ptychography with a convex relaxation," *New journal of physics*, vol. 17, no. 5, p. 053044, 2015.

[33] S. Marchesini, H. He, H. N. Chapman, S. P. Hau-Riege, A. Noy, M. R. Howells, U. Weierstall, and J. C. Spence, "X-ray image reconstruction from a diffraction pattern alone," *Physical Review B*, vol. 68, no. 14, p. 140101, 2003.

[34] H. N. Chapman, A. Barty, M. J. Bogan, S. Boutet, M. Frank, S. P. Hau-Riege, S. Marchesini, B. W. Woods, S. Bajt, W. H. Benner *et al.*, "Femtosecond diffractive imaging with a soft-x-ray free-electron laser," *Nature Physics*, vol. 2, no. 12, pp. 839–843, 2006.

[35] G. Oszlányi and A. Sütő, "The charge flipping algorithm," *Acta Crystallographica Section A: Foundations of Crystallography*, vol. 64, no. 1, pp. 123–134, 2008.

[36] M. L. Moravec, J. K. Romberg, and R. G. Baraniuk, "Compressive phase retrieval," in *Optical Engineering+ Applications*. International Society for Optics and Photonics, 2007, pp. 670 120–670 120.

[37] S. Marchesini, "Ab initio undersampled phase retrieval," *Microscopy and Microanalysis*, vol. 15, no. S2, pp. 742–743, 2009.

[38] H. Ohlsson, A. Yang, R. Dong, and S. Sastry, "Cprl–an extension of compressive sensing to the phase retrieval problem," in *Advances in Neural Information Processing Systems*, 2012, pp. 1367–1375.

[39] X. Li and V. Voroninski, "Sparse signal recovery from quadratic measurements via convex programming," *SIAM Journal on Mathematical Analysis*, vol. 45, no. 5, pp. 3019–3033, 2013.

[40] S. Mukherjee and C. S. Seelamantula, "Fienup algorithm with sparsity constraints: application to frequency-domain optical-coherence tomography," *IEEE Transactions on Signal Processing*, vol. 62, no. 18, pp. 4659–4672, 2014.

[41] Z. Yang, C. Zhang, and L. Xie, "Robust compressive phase retrieval via l1 minimization with application to image reconstruction," *arXiv preprint arXiv:1302.0081*, 2013.

[42] Y. Shechtman, A. Beck, and Y. C. Eldar, "Gespar: Efficient phase retrieval of sparse signals," *Signal Processing, IEEE Transactions on*, vol. 62, no. 4, pp. 928–938, 2014.

[43] P. Schniter and S. Rangan, "Compressive phase retrieval via generalized approximate message passing," *IEEE Transactions on Signal Processing*, vol. 63, no. 4, pp. 1043–1055, 2015.

[44] S. Loock and G. Plonka, "Phase retrieval for fresnel measurements using a shearlet sparsity constraint," *Inverse Problems*, vol. 30, no. 5, p. 055005, 2014.

[45] H. Chang, Y. Lou, M. Ng, and T. Zeng, "Phase retrieval from incomplete magnitude information via total variation regularization," *SIAM Journal on Scientific Computing (See CAM Report No. 16-39)*, vol. to appear.

[46] H. Chang, Y. Lou, and Y. Duan, "Total variation based phase retrieval for poisson noise removal," *UCLA CAM Report*, vol. 16-76.

[47] A. M. Tillmann, Y. C. Eldar, and J. Mairal, "Dolphin-dictionary learning for phase retrieval," *arXiv preprint arXiv:1602.02263*, 2016.

[48] T. Qiu and D. P. Palomar, "Undersampled phase retrieval via majorization-minimization," *arXiv preprint arXiv:1609.02842*, 2016.

[49] C. Wu and X.-C. Tai, "Augmented Lagrangian method, dual methods and split-Bregman iterations for ROF, vectorial TV and higher order models," *SIAM J. Imaging Sci.*, vol. 3, no. 3, pp. 300–339, 2010.

[50] S. Boyd, N. Parikh, E. Chu, B. Peleato, and J. Eckstein, "Distributed optimization and statistical learning via the alternating direction method of multipliers," *Foundations and Trends® in Machine Learning*, vol. 3, no. 1, pp. 1–122, 2011.

[51] S. V. Venkatakrishnan, C. A. Bouman, and B. Wohlberg, "Plug-and-play priors for model based reconstruction," in *Global Conference on Signal and Information Processing (GlobalSIP), 2013 IEEE*. IEEE, 2013, pp. 945–948.

[52] F. Li and T. Zeng, "A universal variational framework for sparsity-based image inpainting," *IEEE Transactions on Image Processing*, vol. 23, no. 10, pp. 4242–4254, 2014.

[53] B. He, H. Liu, Z. Wang, and X. Yuan, "A strictly contractive peaceman–rachford splitting method for convex programming," *SIAM Journal on Optimization*, vol. 24, no. 3, pp. 1011–1040, 2014.

[54] S. Osher and L. I. Rudin, "Feature-oriented image enhancement using shock filters," *SIAM Journal on Numerical Analysis*, vol. 27, no. 4, pp. 919–940, 1990.

[55] L. Alvarez, P.-L. Lions, and J.-M. Morel, "Image selective smoothing and edge detection by nonlinear diffusion. ii," *SIAM Journal on numerical analysis*, vol. 29, no. 3, pp. 845–866, 1992.

[56] R. Malladi and J. A. Sethian, "Image processing via level set curvature flow," *proceedings of the National Academy of sciences*, vol. 92, no. 15, pp. 7046–7050, 1995.

[57] L. I. Rudin, S. Osher, and E. Fatemi, "Nonlinear total variation based noise removal algorithms," *Physica D: Nonlinear Phenomena*, vol. 60, no. 1, pp. 259–268, 1992.

[58] J. Lie, M. Lysaker, and X.-C. Tai, "A variant of the level set method and applications to image segmentation," *Math. Comp.*, vol. 75, pp. 1155–1174, 2006.

[59] K. Bredies, K. Kunisch, and T. Pock, "Total generalized variation," *SIAM Journal on Imaging Sciences*, vol. 3, no. 3, pp. 492–526, 2010.

[60] X.-C. Tai, J. Hahn, and G. J. Chung, "A fast algorithm for euler's elastica model using augmented lagrangian method," *SIAM Journal on Imaging Sciences*, vol. 4, no. 1, pp. 313–344, 2011.

[61] A. Danielyan, V. Katkovnik, and K. Egiazarian, "Bm3d frames and variational image deblurring," *IEEE Transactions on Image Processing*, vol. 21, no. 4, pp. 1715–1728, 2012.

[62] A. Rond, R. Giryes, and M. Elad, "Poisson inverse problems by the plug-and-play scheme," *arXiv preprint arXiv:1511.02500*, 2015.

[63] M. Lysaker, A. Lundervold, and X.-C. Tai, "Noise removal using fourth-order partial differential equation with applications to medical magnetic resonance images in space and time," *IEEE Transactions on image processing*, vol. 12, no. 12, pp. 1579–1590, 2003.

[64] X. Zhang, M. Burger, X. Bresson, and S. Osher, "Bregmanized nonlocal regularization for deconvolution and sparse reconstruction," *SIAM Journal on Imaging Sciences*, vol. 3, no. 3, pp. 253–276, 2010.

[65] C. Tomasi and R. Manduchi, "Bilateral filtering for gray and color images," in *Computer Vision, 1998. Sixth International Conference on*. IEEE, 1998, pp. 839–846.

[66] A. Buades, B. Coll, and J.-M. Morel, "Image denoising methods. a new nonlocal principle," *SIAM review*, vol. 52, no. 1, pp. 113–147, 2010.

[67] K. Dabov, A. Foi, V. Katkovnik, and K. Egiazarian, "Image denoising by sparse 3-d transform-domain collaborative filtering," *Image Processing, IEEE Transactions on*, vol. 16, no. 8, pp. 2080–2095, 2007.

[68] F. Li and T. Zeng, "A new algorithm framework for image inpainting in transform domain," *SIAM Journal on Imaging Sciences*, vol. 9, no. 1, pp. 24–51, 2016.

[69] C. A. Metzler, A. Maleki, and R. G. Baraniuk, "Bm3d-prgamp: Compressive phase retrieval based on bm3d denoising," in *Image Processing (ICIP), 2016 IEEE International Conference on*. IEEE, 2016, pp. 2504–2508.

[70] C. Wu, J. Zhang, and X.-C. Tai, "Augmented lagrangian method for total variation restoration with non-quadratic fidelity," *Inverse problems and imaging*, vol. 5, no. 1, pp. 237–261, 2011.

[71] Wolfram, "CubicFormula," http://mathworld.wolfram.com/CubicFormula.html.

[72] P. Milanfar, "A tour of modern image filtering: New insights and methods, both practical and theoretical," *IEEE Signal Processing Magazine*, vol. 30, no. 1, pp. 106–128, 2013.

[73] T. Goldstein and S. Osher, "The split bregman method for l1-regularized problems," *SIAM Journal on Imaging Sciences*, vol. 2, no. 2, pp. 323–343, 2009.

[74] G. Gilboa and S. Osher, "Nonlocal operators with applications to image processing," *Multiscale Modeling & Simulation*, vol. 7, no. 3, pp. 1005–1028, 2008.

[75] S. H. Chan, X. Wang, and O. A. Elgendy, "Plug-and-play admm for image restoration: Fixed point convergence and applications," *arXiv preprint arXiv:1605.01710*, 2016.